CORA Cork Open Research Archive
Cartlann Taighde Oscailte Chorcaí

Title	Formation mechanism of metal–molecule–metal junctions: molecule-assisted migration on metal defects
Authors	Thompson, Damien;Liao, Jianhui;Nolan, Michael;Quinn, Aidan J.;Nijhuis, Christian A.;O'Dwyer, Colm;Nirmalraj, Peter N.;Schönenberger, Christian;Calame, Michel
Publication date	2015-08-05
Original Citation	Thompson, D., Liao, J., Nolan, M., Quinn, A. J., Nijhuis, C. A., O'Dwyer, C., Nirmalraj, P. N., Schönenberger, C. and Calame, M. (2015) 'Formation Mechanism of Metal–Molecule–Metal Junctions: Molecule-Assisted Migration on Metal Defects', The Journal of Physical Chemistry C, 119(33), pp. 19438-19451. doi: 10.1021/acs.jpcc.5b04383
Type of publication	Article (peer-reviewed)
Link to publisher's version	http://pubs.acs.org/doi/abs/10.1021/acs.jpcc.5b04383 - 10.1021/acs.jpcc.5b04383
Rights	© 2015 American Chemical Society. This document is the Accepted Manuscript version of a Published Work that appeared in final form in The Journal of Physical Chemistry C, copyright © American Chemical Society after peer review and technical editing by the publisher. To access the final edited and published work see https://pubs.acs.org/doi/abs/10.1021/acs.jpcc.5b04383
Download date	2026-11-04 21:55:52
Item downloaded from	https://hdl.handle.net/10468/6573



University College Cork, Ireland
Coláiste na hOllscoile Corcaigh

Formation Mechanism of Metal−Molecule−Metal Junctions: Molecule-Assisted Migration on Metal Defects

Damien Thompson,*[,†] Jianhui Liao,[‡,§] Michael Nolan,[∥] Aidan J. Quinn,[∥] Christian A. Nijhuis,[⊥,#] Colm O'Dwyer,[∥,▽] Peter N. Nirmalraj,[○] Christian Schönenberger,[‡] and Michel Calame[‡]

[†]Department of Physics and Energy and Materials and Surface Science Institute, University of Limerick, Ireland

[‡]Department of Physics and Swiss Nanoscience Institute, University of Basel, Klingelbergstrasse 82, CH-4056 Basel, Switzerland

[§]Key Laboratory for the Physics and Chemistry of Nanodevices, Department of Electronics, Peking University, Beijing, P.R. China

[∥]Micro/Nanoelectronics Centre, Tyndall National Institute, Dyke Parade, University College Cork, Cork, Ireland

[⊥]Department of Chemistry, National University of Singapore, 3 Science Drive 3, Singapore 117543

[#]Graphene Research Centre, National University of Singapore, 2 Science Drive 3, Singapore 117542

[▽]Applied Nanoscience Group, Department of Chemistry, University College Cork, Cork, Ireland

[○]IBM Research − Zürich, Saumerstrasse 4, CH-8803 Rüschlikon, Switzerland

ABSTRACT

Activation energies, E_a, measured from molecular exchange experiments are combined with atomic-scale calculations to describe the migration of bare Au atoms and Au−alkanethiolate species on gold nanoparticle surfaces during ligand exchange for the creation of metal−molecule−metal junctions. It is well-known that Au atoms and alkanethiol−Au species can diffuse on gold with sub-1 eV barriers, and surface restructuring is crucial for self-assembled monolayer (SAM) formation for interlinking nanoparticles and in contacting nanoparticles to electrodes. In the present work, computer simulations reveal that naturally occurring ridges and adlayers on Au(111) are etched and resculpted by migration of alkanethiolate−Au species toward high coordination kink sites at surface step edges. The calculated energy barrier, E_b, for diffusion via step edges is 0.4−0.7 eV, close to the experimentally measured E_a of 0.5−0.7 eV. By contrast, putative migration from isolated nine-coordinated terrace sites and complete Au unbinding from the surface incur significantly larger barriers of +1 and +3 eV, respectively. Molecular van der Waals packing energies are calculated to have negligible effect on migration barriers for typically used molecules (length < 2.5 nm), indicating that migration inside SAMs does not change the size of the migration barrier. We use the computational methodology to propose a means of creating Au nanoparticle arrays via selective replacement of citrate protector molecules by thiocyanate linker molecules on surface step sites. This work also outlines the possibility of using Au/Pt alloys as possible candidates for creation of contacts that are well-formed and long-lived because of the superior stability of Pt interfaces against atomic migration.

INTRODUCTION

The relentless miniaturization of interconnects down to widths of a few nanometers has increased the practical significance of metal atom migration in electronic devices.[1] In addition, electromigration has been intensely studied in recent years as a possible route toward near atom-scale control in the wafer-scale fabrication of noble metal nanostructures[2−7] that can be contacted by molecules to form molecular tunnel junctions by bridging two nanoparticles. These junctions can be used to form extended arrays of nanoparticles,[8−11] which permit the fabrication of a large number of junctions in parallel and represent a valuable platform for testing the features of molecular-scale circuits.[12,13] The rational design of reliable, efficient metal−molecule contacts requires knowledge of the atomic-level motion of atoms in the metal, molecules, and chemical binding events underlying the formation of metal−molecule contacts and, eventually, junctions. Better contacts will in turn aid the development of materials that provide self-assembled, stable molecular tunnel junctions. Atomic resolution scanning tunnelling microscopy (STM) data of surface migration and reconstructions is rare but becoming more available for metals and metal oxides; see, e.g., the alkanethiolate−Au(111) surface structure resolved in ref 14 and oxygen defect dynamics in manganite monitored as described in ref 15.

The determination of conductance paths through tunnel junctions has received much attention in recent years.[16−27] The present study focuses instead on developing a more detailed

picture of junction assembly, in particular rearrangements in the local gold structure, crucial for the refinement of mechanical break junctions, electromigration junctions, and molecule-linked arrays of nanoparticles. In the present work, activation energies are deduced from molecular exchange experiments, and this experimental data is combined with calculated migration barriers to propose a detailed model for coupled gold atom migration and molecule self-assembly in junction formation. We use first-principles calculations to compute the energy barrier for diffusion of gold atoms and Au−alkanethiolate species over a range of surface structures, providing estimated thermodynamic penalties for the different stages of dissociation, from low-barrier migration, or rolling, through to complete unbinding. Our data and analysis complements recent STM studies of molecule-induced rearrangements and adatom migration on gold,[14,28−33] which investigate the effect of surface features including grain boundaries and pores.[20,34]

We calculate a barrier of 3 eV for complete gold atom unbinding, consistent with the upper bound of literature values that range from approximately 1 to 3 eV,[35−37] depending on the method used to estimate binding strengths. By contrast, for gold atom migration via exchange between partially bound arrangements on step edges, termed rolling or "hopping",[4] we compute sub-1 eV barriers, similar to the sub-1 eV hopping barriers estimated from microscopy experiments,[38,39] and significantly lower than the barrier to complete unbinding. As well as junction formation, such low-energy migration may also be involved in defect healing and gold ad-layer formation.[40,41] We combine the computed gold migration barriers with computed molecule packing energies on Au(111) and Au_{20} nanoparticles and experiments on the creation of molecule-linked nanoparticle arrays (measured activation energy $E_a = 0.6 \pm 0.1$ eV, in good agreement with the density functional theory (DFT) calculations), to develop a more complete picture of gold atom migration in molecular junction assembly. Intermolecular packing energies remain smaller than the calculated migration energies for molecule lengths up to 18 carbons, indicating that close-packed self-assembled monolayer (SAM) regions do not raise the migration barrier for typically used, sub-C18 alkanethiolate chain lengths.

Harnessing concerted metal atom and molecule dynamics may allow better control of SAM and junction creation for, e.g., nanoparticle functionalization and interlinking.[42,43] To this end, the data presented in this study complements earlier computational scans of the Au−S bond strength at structurally inequivalent Au_{20} (and Au_{55}) sites[44] and allows us to propose a means of linking gold nanoparticles (creating *n*-mers) by replacing a small population of the commonly used protector molecules of trisodium citrate with a rhenium-based thiocyanate (NCS) linker. The *n*-mers can be formed by mixing citrate-stabilized nanoparticles with the di-isothiocyanate molecules. Our calculations show that di-isothiocyanate molecules bind to step sites on the nanoparticles, and we propose that this will enable the nanoparticles to link together to form clusters in solution. While the binding energetics and molecular dynamics of thiol-functionalized gold nanoparticles have been the subject of intense study in recent years, with some consensus and also some remaining open questions,[45−57] this study is to the authors's knowledge the first to compute the binding energetics of citrates and organometallic di-isothiocyanate linkers on gold surfaces. Two recent studies used a combination of quantum mechanics and molecular dynamics to support spectroscopy and microscopy characterizations for two related phenomena.[58,59] The first[58] described the exchange of cysteine, the amino acid with a thiol side chain, and citrates on gold, though focused mainly on citrate−linker interactions rather than explicit calculation of citrate versus linker binding strengths to gold, while the second[59] used gold−thiol, and in earlier work silver-citrate,[60] binding strengths and water-mediated surface dynamics interactions to propose novel nanoparticle growth mechanisms. The importance of atom-scale approaches, and the corresponding limitations of purely mesoscopic theories, to describe mixed monolayers on nanoparticles has been emphasized in a comprehensive survey of nanoparticle solubility[61] and, more generally, monolayer-mediated interfacial energies.[62]

MATERIALS AND METHODS

This section contains further technical details on the experimental methods and simulation protocols used; the main features of the measurements and models are summarized in Results.

Experiments. Two-dimensional arrays of octanethiol-coated 10 nm diameter nanoparticles were prepared via self-assembly and transferred to a SiO_2/Si wafer for subsequent contacting using lithography techniques.[63,64] This process provides tens of devices, each typically comprising more than 10^6 nanoparticles arranged in a hexagonally close-packed array. The alkanethiolate layer ensures spacing between neighboring nanoparticles in the nanometer range. Using a molecular exchange process where incoming dithiolated compounds can partially displace the alkanethiolates, we can interconnect neighboring nanoparticles to form an array of molecular junctions.[8−10] To perform a molecular exchange at three distinct temperatures of 0, 25, and 40 °C, we immersed each substrate in an Ar-bubbled 1 mM THF solution of oligo (*p*-phenylene ethynylene) dithiol, for short OPE-dithiol molecules. After a well-defined time interval, the substrate was taken out of the solution, rinsed, dried in a N_2 flow, and measured in ambient. The next exchange step was then started, and the process was repeated. The time intervals ranged between 5 min and ∼1 day.

During the exchange process, octanethiols are progressively replaced by OPE-dithiols, and more and more molecular junctions, with a relatively high local conductance, are formed.[63] Once a continuous path of OPE-bridged junctions runs from source to drain, conductance, *G*, rises dramatically. The general behavior of the curves, i.e., fast conductance increase followed by saturation, appears quite universal in Figure 1, with a marked effect due to the temperature. The specific microscopic details of the nanoparticle assemblies lead to slight device-to-device conductance differences, as reported previously.[63,64]

Calculations. Three levels of atomic scale calculations are used to describe the atom-scale mechanisms of gold surface rearrangements, namely, two types of electronic structure calculations and classical molecular dynamics simulations. First, two types of quantum mechanical models, periodic surface models and molecular clusters, were used to compute the migration energies over a range of different gold surface sites. The combination of the periodic surface models and molecular models allowed us to sample a wide range of different surface coordination states. SAM molecule−molecule van der Waals interaction strengths were calculated using classical molecular dynamics simulations of alkanethiolate-passivated gold.

Periodic Calculations. The periodic surface models were described using periodic plane wave DFT in the VASP code[65] with the GGA-PBE functional,[66] projector augmented wave (PAW)[67] pseudopotentials with a plane wave cutoff of 400 eV, and Brillouin zone Γ-point sampling. We used a ∼220-atom slab for Au(111) with 30 Å vacuum spacing. A 224-atom slab incorporated a typical step edge defect, while a 216-atom slab featured a two-layer, apexed ridge (Figure 2). All atoms were allowed to relax unconstrained until the forces on each atom were <3 meV/Å. While our computed migration energies are converged to <10 meV with respect to plane wave cutoff, *k*-point sampling, model size, and vacuum spacing, we note that other authors (see, e.g., refs 68 and 69) have used smaller models but denser *k*-point grids to probe the fine details of surface bonding, dipole, and work function shifts beyond the scope of this study. Further details of the periodic surface models are in section S1 of Supporting Information.

Cluster Calculations. The use of periodic and cluster models for the calculation of surface migration energies allows a wide sampling of surface sites and, in the instances where different models were used to describe the same type of site, each model type gives a similar migration energy allowing direct qualitative comparison between migration energies calculated for the different types of structurally inequivalent gold nanocrystal surface sites, going from coordinatively saturated "terrace" surface sites to progressively more coordinatively unsaturated "step edge", "ridge", and "apex" surface sites.

The tetrahedral Au_{20} cluster was generated from the bulk Au crystal structure, and its optimized geometry and electronic structure were calculated using the Gaussian03 code[70] with the B3LYP[71] hybrid Hartree−Fock DFT wave function and the relativistic LANL2DZ basis set. Geometries were optimized via nuclear relaxation to root-mean-square (RMS) atomic forces and displacements below 0.0003 atomic units and 0.0012 atomic units, respectively. The Au_{20} cluster has four faces, each representing a (111) surface of face-centered cubic (fcc) gold and provides a computationally feasible approximation to the cuboctahedral Au_{55} (111) faces,[72] given the 40+ optimizations required for the present study. Nine-coordinated terrace, six-coordinated ridge, and three-coordinated apex site atoms are provided by the three different coordination sites in the T_d structure, with four atoms at the center of each face, 12 along the edges and 4 at the tips. For computational simplicity, the calculations measure rebinding because the fully bound complex will not spontaneously dissociate in the simulations; therefore, the curves "start" at large displacement and end in fully bound complexes. Each curve comprises 70−120 data points generated from ∼10 different starting geometries whereby one gold atom is displaced from a terrace, ridge, or apex site with increasingly large starting displacements (reading the plots in Figure 4 from left to right) taken along a vector perpendicular to the binding plane. The path of reapproach of the displaced Au atom is then calculated from the DFT structures and energies. The data points overlay very well between different starting structures to provide the smooth curves in Figure 4. Control simulations were performed on alternative prolate Au_{20} cluster geometries, Au_{20}:Au_{20} grain boundaries, and platinum clusters, as described in section S4.2 of Supporting Information.

Calculations of Au_{19} defect clusters (described in detail in section S3.3) were performed in a similar way, using the Gaussian03 code[70] with the B3LYP[71] wave function and LANL2DZ basis set, and preserved the net neutrality of the cluster.[73] The dissociation energy was calculated in the usual way, by subtracting the electronic energy of the [Au_{19} + Au] separated system from that of the fully bound reference Au_{20} cluster. Electron density and molecular orbital surfaces were produced using MOLEKEL Unix version 4.3.[74] Overlaid structure images and movies were produced using MOLDEN Unix version 4.7[75] and VMD Unix version 1.8.7.[76] The input scripts used for the simulations, together with the computed structures, are available on request from the corresponding author.

We note that the DFT binding potentials computed in the present work provide an estimate of the force-dependent activation barrier, E_a, in the overall Arrhenius expression.[77] Hence, the experimentally observed rupture forces are a function of the intrinsic gold−gold interaction strengths measured by DFT together with the temperature and any applied external force, electrical or otherwise (e.g., chemical or mechanical). For example, during electromigration, the local temperature in gold junctions can rise as high as ∼450 K.[78]

To put the 3 eV dissociation and sub-1 eV migration barriers computed in the main text in context, recent calculations of gold adatom diffusion have indicated also a low, sub-1 eV barrier for migration on another gold surface, in this case Au(100),[79] and similarly small barriers were used in early molecular dynamics studies of gold diffusion on copper and gold surfaces.[80,81] Recent calculations of Au atom diffusion on graphene have found a 1.4 eV barrier to migration along the sheet edge.[82]

Molecular Dynamics Simulations. During the development of the thermodynamic model for gold−molecule−gold junction assembly in gold nanoparticle interlinking, the other major energy component, apart from resculpting of the gold surfaces, is the bulk van der Waals packing interaction between the molecules, which are typically alkanethiolate chains but can also be, e.g., alkyl amines[83] or oligo(*p*-phenylene ethylene) (OPE) molecules.[64] These stabilizing interactions are lost or reduced when a single molecule or a small cluster of molecules come out of bulk solution to form a junction and cost ∼0.05−0.10 eV per methylene unit, as estimated from molecular dynamics simulations[84] using the CHARMM force field[85] for alkanethiol molecules in bulk liquid and self-assembled monolayer (SAM) environments. More details are in section S4.3 of Supporting Information.

RESULTS

We first describe experiments that provide an estimate of the activation energy, E_a, for molecular exchange at gold junctions and then present electronic structure calculations of gold atom diffusion on gold surfaces and gold clusters. The migration barriers, E_b, computed from the electronic structure calculations are used to rationalize the experimental measurements. The full modeling data set (details are in Supporting Information) measures alkanethiolate−Au and single Au atom migration barriers on Au(111) terrace, step edge, and ridge sites, together with migration energies on discrete (Au and Pt) nanoparticles and at grain boundaries. To estimate the contribution to E_b from molecule−molecule packing interactions, we report calculated molecule-in-SAM packing energies on Au(111) and Au_{20} nanoparticles for alkanethiolates and a range of other molecules commonly used in metal−molecule junctions. Finally, we present the energetics of selective replacement of thiocyanate linkers on citrate-protected Au nanoparticle surfaces.

Experimental Estimates of Contact Formation Energy. Experiments taking advantage of a molecular exchange process bring additional insight into the energetics of gold migration for contact formation in molecular junctions. A detailed description of the experimental methods is provided in Materials and Methods. Briefly, we fabricate arrays of octanethiol-coated gold nanoparticles using self-assembly, microcontact printing, and lithography techniques.[8−11] By performing a molecular exchange process with oligo (*p*-phenylene ethynylene) dithiol, we interconnect neighboring nanoparticles to form an array of molecular junctions.[8−11,63] Figure 1a shows a SEM image of a

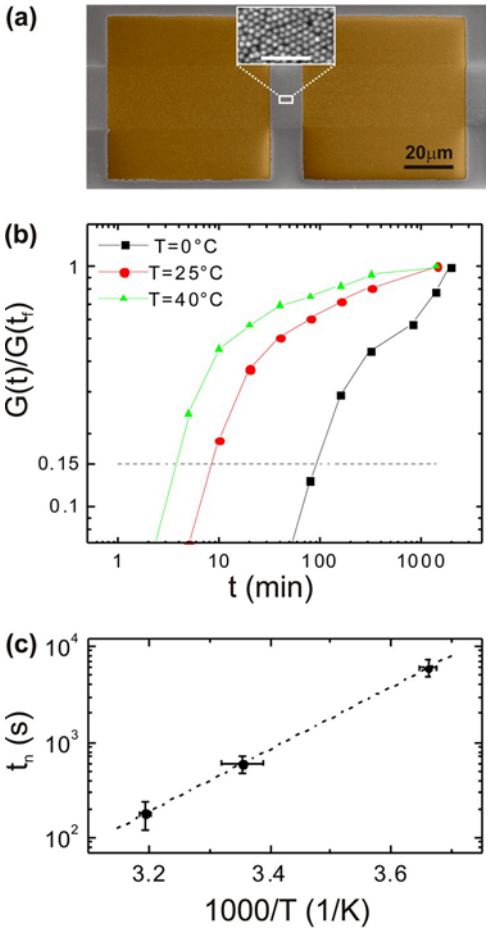


Figure 1. (a) Scanning electron microscopy (SEM) micrograph of a nanoparticle array line transferred to a SiO_2/Si substrate and contacted with gold pads (colored in yellow). The inset shows a higher magnification SEM image revealing the hexagonal arrangement of the Au nanoparticles. Scale bar: 100 nm. (b) Normalized conductance, $G(t)/G(t_f)$, versus time, t, during molecular exchange at T = 0 °C (black squares), 25 °C (red circles), and 40 °C (green triangles). t_f is the final time of the experiment at each temperature. A typical time scale $t_n(T)$ for the exchange at each temperature is taken at a normalized conductance value of 0.15 (horizontal dashed line). (c) Arrhenius plot of $t_n(T)$. The activation energy, E_a, deduced from the linear fit corresponds to 0.6 ± 0.1 eV.

typical device after molecular exchange where two gold electrodes (colored yellow) contact a nanoparticle array. We performed molecular exchange at three distinct temperatures: 0, 25, and 40 °C. The conductance, G, for ten devices was monitored as a function of time, t, during the exchange at all three temperatures. We note that some of the data presented here has also been very recently analyzed in the context of a percolation study discussed in ref 11.

In Figure 1b, we show the conductance $G(t)$ (normalized to the final conductance value $G(t_f)$ at the end of the exchange) versus time, for the three temperatures investigated. Each data point is the value of the normalized conductance $G(t)/G(t_f)$ averaged over 10 devices measured at each temperature. The data show that the exchange kinetics is strongly temperature-dependent and suggest a similar mechanism at all temperatures: after a rapid conductance increase of up to 2 orders of magnitude,[63] the curves tend to flatten and saturate. We observe that full saturation has not been reached at 0 °C even though we prolonged the exchange for 30 h. The raw data for the molecular exchange at all three temperatures are shown in the Figure S0 of Supporting Information.

To estimate the energy barrier involved in the junction formation upon molecular exchange, we extract for each temperature a typical time, $t_n(T)$, such that $G(t)/G(t_f) = 0.15$ at $t = t_n$ (horizontal dashed line in Figure 1b). An Arrhenius plot for $t_n(T)$ is shown in Figure 1c. For a thermally activated process dominated by a single energy barrier, we can write $(t_n/T) = (t_0/T)\exp(-E_a/k_BT)$ where (t_0/T) is a temperature-dependent attempt frequency and E_a is the activation energy barrier. We extract the energy barrier, E_a, from the slope of the $t_n(T)$ versus $1/T$ graph. A linear fit to this data yields an activation energy for the exchange process of about (6 ± 1) × 10^4 J/mol. This corresponds to $E_a = 0.6 \pm 0.1$ eV per molecule. The normalized conductance value of 0.15 to determine t_n was chosen rather arbitrarily. This is due to the fact that we cannot access the inflection point of the exchange curve; the onset of the exchange is too fast to obtain reliable data in time intervals below a few minutes. We emphasize that the activation energy value obtained does not vary noticeably if we change this $G(t)/G(t_f) = 0.15$ criterion. Using values for $G(t)/G(t_f)$ ranging between 0.1 and 0.4, we observe that the extracted $t_n(T)$ values give activation energies ranging between 0.57 and 0.65 eV. The choice of $G(t)/G(t_f)$ therefore does not play a significant role in the analysis. The value found for the activation energy compares well with the 0.7 eV found from conducting atomic force microscopy studies[86] where the thermally activated breakdown of alkanethiolate−Au junctions was investigated. We expect the molecular bridging of adjacent nanoparticles to be a multistep process. From the data in Figure 1, we can infer that a thermally activated process with an energy barrier around 0.6 eV seems to be the dominant, rate-limiting step in this process. We will show below that this energy barrier obtained experimentally is consistent with the 0.4−0.7 eV migration barriers, E_b, computed for alkanethiolate−Au moieties on gold step edges.

Gold Atom and Alkanethiolate−Au Molecule Migration on a Au(111) Surface Containing a Range of Naturally Occurring Defects. We use a combination of periodic and cluster models to simulate gold atom migration and compare the calculated energy barriers with the experimental measurements of activation energies at metal−molecule junctions. Both types of models have advantages and disadvantages. While cluster models[44,72,73,87] such as Au_{20} and Au_{55} can provide realistic representation of the local features of the tip apex of a sharp gold electrode,[88] the size of molecular clusters is generally far smaller than the few nanometer diameter nanoparticles and the extended junction surface (e.g., a 10 nm diameter Au nanoparticle contains on the order of 30 000 atoms, given the density of bulk face-centered cubic

(fcc) Au of 59 atoms/nm^3). Hence, the small Au_{20} clusters allowed us to perform a large number of detailed calculations to track the migration path of gold atoms from a variety of surface binding sites (as described in Crumbling, Atomic Migration, and Sculpting of Gold Clusters). Because Au_{20} is a molecular cluster with a HOMO−LUMO gap, a separate periodic slab model of Au(111) that maintains the metallicity of the surface was used to measure migration of Au atoms on the gold surface. These periodic simulation cells include a range of experimentally observed, naturally occurring surface features (see refs 28−31 and references cited therein) such as terraces, step edges, and ridges and provide a realistic extended surface model on which to compute gold atom migration barriers.

A second set of periodic models were used to include the bound alkanethiolate molecule and allow a direct calculation of the effect of alkanethiolate binding on gold atom migration and the migration barrier for the alkanethiolate−Au moiety on the gold surface. Figure 2 shows illustrative examples of the surface models used to calculate the energetics of Au atom and alkanethiolate−Au species migration paths on Au(111). We find barriers E_b of 0.4−0.7 eV, consistent with the experimental E_a, for the migration of alkanethiolate−Au species along step edges. Migration of alkanethiolate−Au from nearest-neighbor terrace sites up to the step edge has a similarly low E_b of 0.6 eV, which may ensure a steady supply of alkanethiolate−Au species for migration along the step. By contrast, migration of alkanethiolate−Au species and single Au atoms from isolated surface terrace sites carries much higher penalties of +1.3 and +1.2 eV. Thus, naturally occurring surface features provide low-energy migration paths.[89] The migration of single Au atoms along step edges has a computed barrier of +0.7−0.8 eV. The average computed lowering of the gold migration barrier by 0.3 eV for alkanethiolate−Au versus bare Au is in addition to the well-known effect of alkanethiolate bonding on the stability of different morphologies of nanoparticles. (This effect is discussed in more detail in section S4.2 of Supporting Information by comparing the Au_{20} tetrahedral structure (T_d) and the alternative alkanethiolate-stabilized Au_{20} structure composed of a prolate Au_8 core surrounded by four surface Au_3-alkanethiolate$_4$ "staple" motifs.[90]) Taken together, the experimental and simulation data provide compelling evidence for coupled gold (ad)atom motion and ligand binding dynamics in the assembly of stable metal−molecule contacts.[44,88] We note that different thiolate-gold surface structures and diffusion mechanisms have been proposed from simulations and experiment, see, e.g., very recent work in ref 91 and for a recent review see ref 88. We focus primarily here on modeling the simplest mechanisms of single gold atom and alkanethiol-gold species migrating on Au(111). Our computed energetics are consistent with experimentally measured activation energies, but other subthreshold pathways and migrating species, e.g., putative alkanethiol−Au−alkanethiol moiteies, may be present that are kinetically invisible yet important for understanding and fine-tuning the formation of molecular junctions.

Migration energies, ΔE_m, were first estimated by computing the penalty for removal of a Au atom from Au(111). Au atom removal energies were computed by comparing pristine and defect surfaces and simply scaling the energies of defect surfaces by $(N - 1)/N$ to allow direct comparison between models, where N is the total number of surface atoms. This yielded Au atom removal energies of +0.86, +0.36, and +0.22 eV for terrace, step edge, and ridge sites, respectively. Computed surface defect structures are given in Figure S3 of Supporting Information. The increased likelihood of atom hopping out of the 5-coordinated ridge site is reflected in the computed energy difference of −0.14 eV for atom removal from a 5-coordinated ridge versus 7-coordinated step edge site. Atom removal from the step edge site is in turn easier (−0.50 eV energy difference) than removal from the most saturated 9-coordinated terrace site. A more accurate means of calculating migration energies, ΔE_m, involves measuring the energy difference between Au unbinding from the original lattice site and rebinding as an adatom, as illustrated in Figure 2, with computed migration barriers, E_b, plotted in Figure 3. These E_b values include the transition structures identified along the migration pathway and provide an estimate of the overall barrier to diffusion to compare with the experimental E_a value (Figure 1c), as described below.

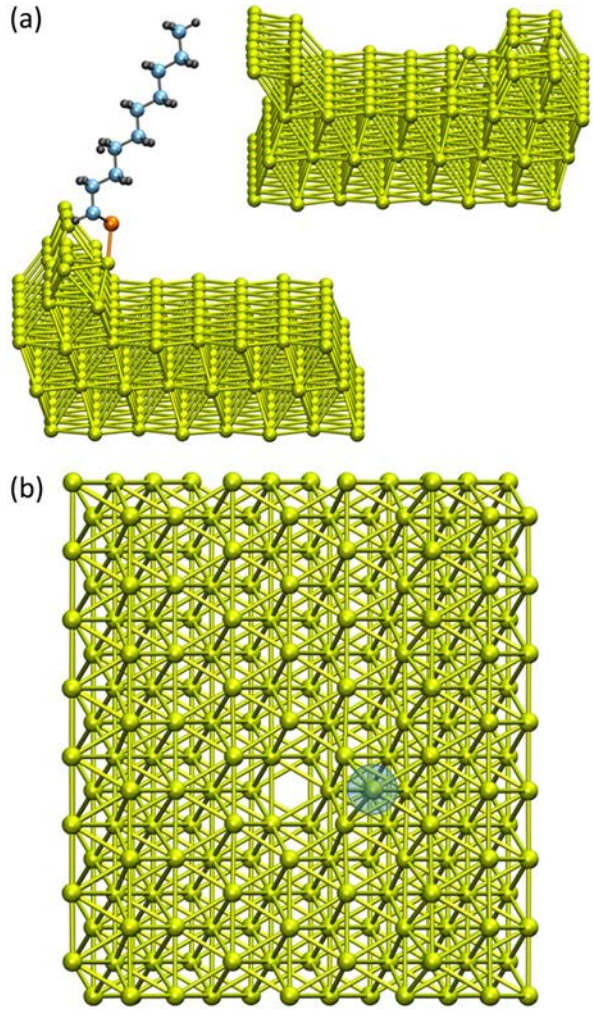


Figure 2. (a) Models showing migration of a Au atom from a step edge site on Au(111) and migration of a Au-$SC_{10}H_{21}$ moiety from a ridge site. The Au atoms rebind as adatom "kinks" on the surface. (b) Top view illustrating migration via hopping of a gold atom up out of a terrace site and rebinding at a step edge defect. These types of models were used to calculate the energetics of migration pathways from terrace, step edge, and ridge sites on Au(111). Bonds are drawn between atoms separated by ≤3.4 Å, and sulfur, carbon, and hydrogen atoms are colored red, blue, and gray, respectively. Images were generated using VMD software.[76] The full set of models is described in section 2 of the Supporting Information.

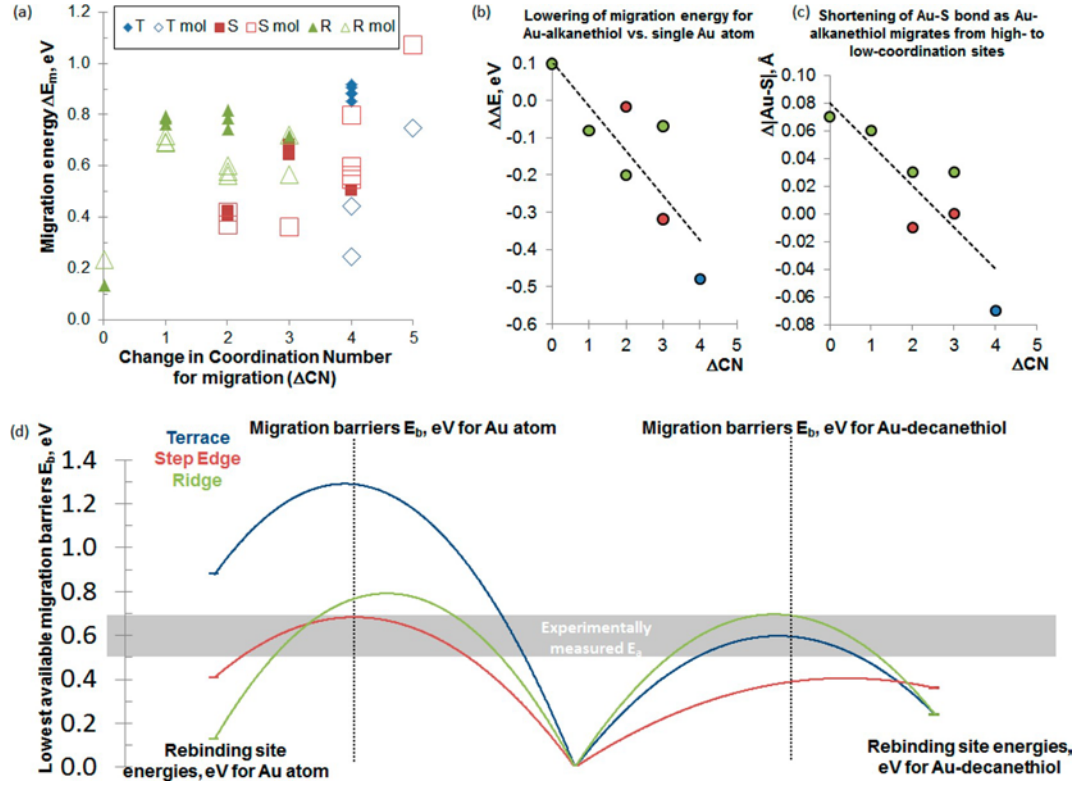


Figure 3. (a) Computed migration energies, ΔE_m, for unbinding and rebinding of single Au atoms and alkanethiolate−Au moieties on Au(111). Higher positive values indicate less stable rebinding sites. In the legend, T, R, and S denote terrace, ridge, and step edge unbinding sites, respectively, and mol indicates migration of a gold atom with a decanethiol molecule covalently bonded to it. Plotted on the horizontal axis is the difference in coordination number of the migrating gold atom in the unbinding site and the coordination number in the site that it rebinds to, ΔCN. Panel b shows the general lowering of migration energies for alkanethiolate−Au versus single Au atom, $\Delta\Delta E_m$, comparing data with the same unbinding site and change in coordination number for rebinding. The line is drawn to guide the eye and shows how the effect of the coordinating molecule becomes more pronounced for migration from high-coordination terrace and step edge sites to low-coordination sites, with associated (c) contraction (strengthening) of Au−S bonds Δ|Au−S|. (d) Migration barrier, E_b, values generated using the data in Figures S4−S10. Computed barriers for Au (left-hand side) and Au−alkanethiolate (right-hand side) in the region of the measured E_a of 0.6 ± 0.1 eV (Figure 1) are marked by the silver shading, to denote possible migration paths taken for surface reorganization in the experiments. Note the "terrace" unbinding site in the models is nearest-neighbor to the step edge feature; more isolated terrace sites have far larger E_b values of +1.3 eV for Au−alkanethiolate diffusion (Figure S7).

The computed E_b values for gold atom hopping out of terrace, step edge, and ridge sites and rebinding on the surface (Figure 3) show a net preference of 0.3 eV for gold migration as part of an alkanethiolate−Au species rather than as a bare gold atom, averaging over all directly comparable models (i.e., same type of unbinding site and same change in coordination number for migration). This lowering of the migration barrier due to molecule binding on the surface reflects the enhanced stability of the migrating gold atom when it is coordinated to the thiol group; indeed, it is generally considered that alkanethiolate molecules migrate and diffuse on metals primarily as alkanethiolate−metal species.[88]

The data in Figure 3 show that the easiest migration of gold is via rolling of alkanethiolate−gold complexes along step edge sites, with low computed barriers consistent with the E_a of +0.6 ± 0.1 eV deduced from the experimental measurements (Figure 1c). We may draw three main conclusions from the combined experimental and simulation data: (1) surface rearrangement for junction formation is made easier by migration of gold atoms with alkanethiolate molecules attached because of the stabilizing effect of the Au−S bond on the migrating Au atom (Figure 3b,c); (2) junction formation can involve extensive migration and surface rearrangements, with the barriers for diffusion between and along ridge and step edge features all consistent with the measured E_a of +0.6 ± 0.1 eV (Figure 3d); and (3) junction formation avoids migration from isolated high-coordination terrace sites (for more on these types of putative high-energy structures, see section S2.2 of Supporting Information). The unusually high stability of alkanethiolate−Au at kinks on step edge sites indicates that these naturally occurring and ubiquitous[28−31] step edge defects provide low-energy paths for migration with E_b = +(0.4−0.7) eV, Figure 3d. Note that bare Au has a relatively low E_b of +0.7 eV on step edges but this rises to +0.8 eV and more sharply to +1.2 eV for migration bridging step edge and, respectively, ridge and terrace sites, emphasizing the stabilizing effect of the coordinating alkanethiolate. Overall, the data in Figure 3d suggest that bare Au atoms can migrate along step edges but require the coordinating alkanethiolate to migrate *to* the step edge.

As described in the next section, the nanoscale roughness of gold surfaces and nanoparticles provides a significant population of low-coordination "glide planes" that provide low-energy pathways for migration. Taken together, the experimental and simulation data indicate that the surface rearrangements required for junction formation involve primarily migration of preformed alkanethiolate−Au species between and along gold surface features. Step edges in

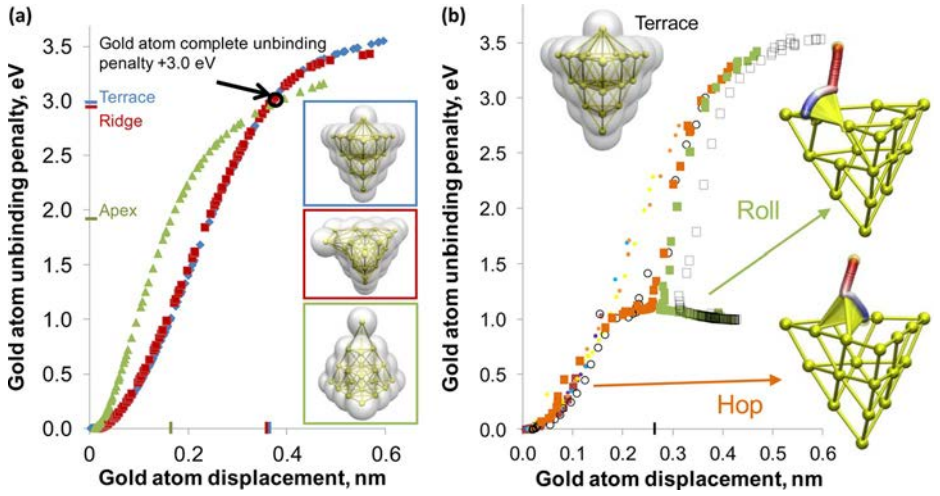


Figure 4. (a) Gold atom unbinding curves showing change in energy as a function of gold atom displacement from terrace, ridge, and apex sites. The intersection of the three curves is labeled and marked by the black circle; the inflection points on each curve are marked on the axes. Partially dissociated gold clusters are shown in the inset panels; the movies included in the Supporting Information (see also section S3.1) show the full range of calculated structures. (b) Migration pathway calculated for the terrace site. This low-energy partial-unbinding pathway involves a hop and then a roll, providing an alternative to the more costly complete unbinding path shown in panel a. The data sets showing the initial hop are marked with hollow black circles and filled orange squares, and the subsequent rolling phase is marked with hollow gray squares and filled green squares. The reference complete unbinding path is marked with small filled circles. The inset panels show the Au hop and roll pathways at either side of the "cusp" at 0.27 nm, as marked on the vertical axis, the separation point at which the atom does one of three things: returns to its original lattice site, rolls on the surface to a new binding site, or completely unbinds. This transition point is just below the lattice Au−Au distance of 0.29 nm. The structures show the diffusing atom colored from red to white to blue as the cluster stabilizes from a dissociated to fully bound state, and the "hinge" motion around the nearest lattice bridge site is illustrated.

particular provide a pathway for migration from high to low coordination sites (e.g., unbinding from 7-coordinated and rebinding at 4-coordinated sites, Figure S8) necessary for formation of tapered metal junctions, which provide strong S−Au binding points[44] and reduced steric repulsions for molecular exchange in nanoparticle interlinking (Figure 1).

Crumbling, Atomic Migration, and Sculpting of Gold Clusters. As described in this section, we find a +1.0 eV barrier to gold atom migration on Au_{20} clusters, similar to the 0.7−1.2 eV range of barriers calculated for single Au atom migration (without the bound alkanethiolate) on Au(111) (Figure 3d). We use the cluster model to (a) more thoroughly explore the conformational space of the migrating gold atom at sub-angstrom resolution and (b) model migration in ultrasmall device components composed of single-nanometer sized metal−molecule−metal contacts. The computed pathways for the complete unbinding of a gold atom from the Au_{20} particle are shown in Figure 4a. The energies on the vertical axis are the energies of perturbed gold clusters relative to the reference fully bonded gold cluster, and displacements on the horizontal axis show the movement of the gold atom away from its "lattice" position. The inset panels of Figure 4a show the cluster model used for the gold particles, the well-known truncated tetrahedral (T_d) twenty-atom gold (Au_{20}) cluster.[73,87] For computational simplicity, the calculations measure rebinding because the fully bound complex will not spontaneously dissociate in the simulations; therefore, the curves "start" at large displacement and end in fully bound complexes. Each curve comprises 70−120 data points generated from ∼10 different starting geometries whereby one gold atom is displaced from a terrace, ridge, or apex site with increasingly large starting displacements (reading the plots in Figure 4a from left to right) taken along a vector approximately perpendicular to the binding site in the cluster. Further simulation details are provided in section S3 of Supporting Information.

We consider gold atom displacements for three cases: (i) a surface atom at the center of a facet (which we term a "terrace" site), (ii) an atom on one vertex (a "ridge" site), and (iii) the atom at the tip ("apex") of the cluster. The unbinding paths in each case are qualitatively similar. We assign an energetic penalty of +3.0 eV for the complete unbinding of a gold atom, from the point at which the three curves intersect in Figure 4a. This intersection point provides a convenient, if rather arbitrary, estimate of the complete unbinding energy as this energy corresponds to displacement of the gold atom in each case by 0.37 nm away from the initial lattice position. This displacement is well beyond the lattice interatomic distance of 1.29 nm, at which point the gold atom is effectively lost to the cluster.

The nine-coordinated terrace and six-coordinated ridge sites exhibit very similar unbinding profiles, with energy rising linearly by ∼1 eV/Å for displacements in the 0.05−0.35 nm range. By contrast, the apex site has a markedly steeper slope up to the inflection point at 0.16 nm displacement, reflecting its steeper potential energy surface for the initial low-displacement phase of unbinding. Further discussion of these coordination-dependent bond stretching penalties is presented in section S3.2 of Supporting Information, with the propensity for unbinding at the different terrace, ridge, and apex sites involving a balance between the number of bonds being broken and the coordination of the atoms around the vacancy that is formed. From the inflection points in Figure 4a, terrace and ridge atoms have very similar energies of 3.0 and 2.9 eV, marking the transition between the steep climb phase of the energy versus displacement curve and the softer final phase of complete unbinding. The three-coordinated apex site has an approximately 1 eV lower inflection point at 1.9 eV, reflecting

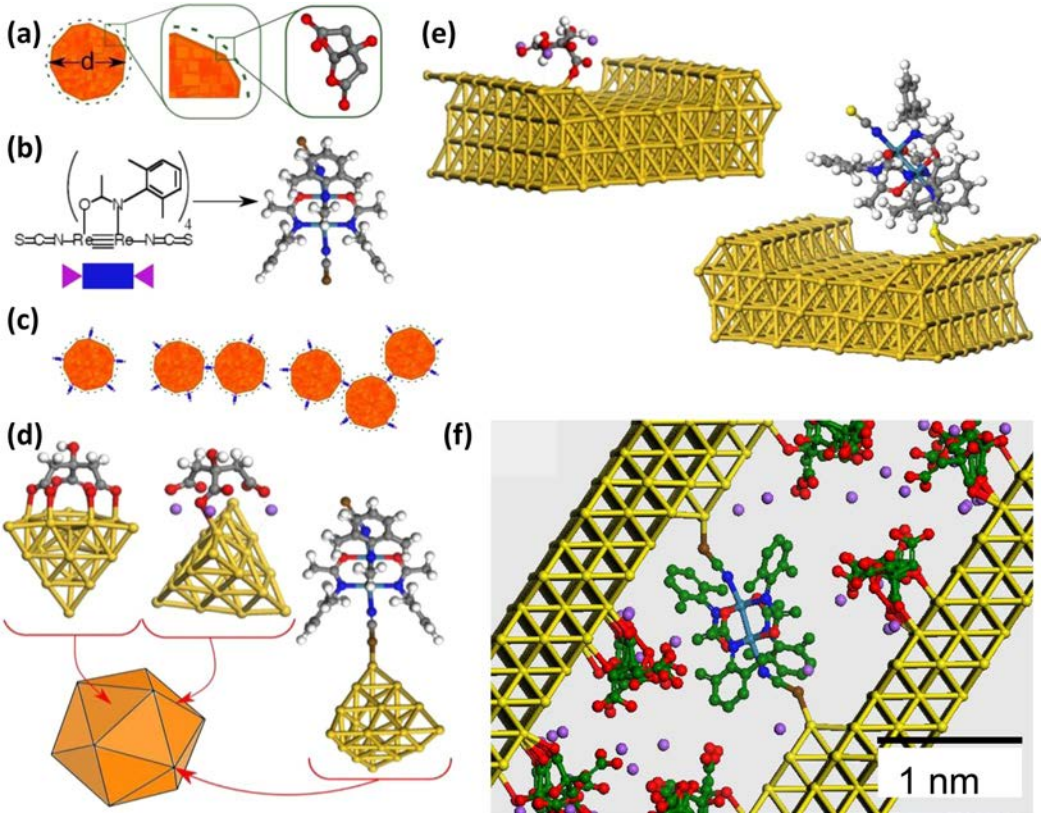


Figure 5. (a) Schematic of a citrate-stabilized gold nanoparticle with core-diameter, d. The molecular structure of the citrate ligand $C_3H_5O(COO)_3^{3-}$ is also shown, where gray and red represent the carbon and oxygen atoms, respectively; hydrogen atoms are not shown. (b) Chemical formula and molecular structure of the proposed organo-metallic di-isothiocyanate linker: $Re_2(DMAA)_4(NCS)_2$, (DMAA = 2,6-dimethylacetanilido); sulfurs are brown, nitrogens blue, and rhenium atoms navy; hereafter termed di-isothiocyanate-linker, which is also represented by the blue and pink symbol. (c) Mixing the citrate stabilized nanoparticles with the di-isothiocyanate-linker molecules to form clusters of nanoparticles (n-mers, where n is the number of nanoparticles in the cluster). For the purposes of illustration, only one molecule is shown between the nanoparticles, but it is probable that more than 1 molecule can be between the nanoparticles. (d) Molecular cluster calculations measure binding of citrate protector (with and without sodium counterions, colored purple) and di-isothiocyanate-linker molecules to terrace, ridge, and apex sites. (e) Periodic surface calculations of protector and linker molecule binding to gold. Similar cells were used for classical molecular dynamics simulations of the surfaces in an aqueous environment. (f) Schematic of the proposed linker/protector mixed monolayer that connects gold particles. Here, carbon atoms are colored green and hydrogen atoms are omitted for clarity; the other atoms are colored as in panels a and b.

the lower number of bonds being broken and hence greater overall stability of a 19-atom cluster with the gold removed from a low-coordination apex site,[73] reflected also in the (marginally) lower-energy tail at displacements greater than 0.37 nm. Extrapolation to extreme displacements using Au_{19} defect clusters (with and without long-range corrections) is presented in section S4 of Supporting Information and supports the estimated barrier of +3 eV for complete removal of a gold atom.

Closer examination of the gold unbinding data reveals an additional low-lying energy plateau for the terrace site (shown in Figure 4b, not included in the outline plots for complete unbinding in Figure 4a), which provides some new insights into gold atom diffusion barriers for junction assembly. Figure 4b highlights the near-flat, 0.2 nm wide window at +1.0 eV in which the gold atom moves on an arc around a neighboring lattice bridge site (as shown in the inset panels of Figure 4b and a movie provided as Supporting Information). This low-energy pathway provides a mechanism whereby the atom can hop out of a lattice site and roll along the surface toward the junction tip[4] without becoming fully dissociated. Transmission electron microscopy experiments show clear surface (electro)migration for gold.[92,93] For reference, platinum electrodes appear to require much larger energies for electromigration.[39]

The computed low-energy pathway for gold migration is situated +1.0 eV above the reference energy for the ground-state, fully bonded cluster (Figure 4b), which is similar to the sub-1 eV E_a and E_b values reported above and also gold atom migration barriers estimated from microscopy experiments,[38,39] though closer to the upper, e.g., Prins et al. 0.81 ± 0.08 eV,[39] than the lower bounds, e.g., Strachan et al. 0.22 eV.[38] This is presumably because it is more difficult to displace an atom from a "molecular" cluster than a metallic surface; the full conformational space for atomic rearrangements in Au_{20} T_d (and prolate) clusters is described in sections S3 and S4.3 of Supporting Information. Nevertheless, the computed +1.0 eV barrier is well below the +3.0 eV barrier computed for complete unbinding and, in the context of alkanethiolate-on-gold self-assembled monolayer formation,[94] the 1.0 eV migration barrier is also significantly lower in magnitude than the −1.7 eV S−Au bond strength.[95] This supports the hypothesis that SAM formation proceeds via alkanethiols diffusing[55] and self-assembling as alkanethiolate−Au moieties,[96] with the greater force required for Au−S versus Au−Au rupture revealed by conducting AFM measurements of the conductance plateau

Table 1. Energetics of Molecule−Nanoparticle Binding for Various Surface Binding Sites: "Terrace", "Step", "Ridge", and "Apex"[a]

gold nanoparticle surface site	molecular binding energy (eV)			
	terrace site	step site	ridge site	apex site
bare citrate protector	−1.59[b]	N/A	−1.35[b]	−1.14[b]
trisodium citrate protector	−1.12[b]/−1.23[c]	−0.92[c]	−0.53[b]	−0.95[b]
di-isothiocyante-based linker	−0.16[b]/−0.20[d]/−0.10[c]	−0.40[c]	−0.30[b]	−0.61[b]

[a]Molecular binding energies were computed by comparing the electronic energies of the complex relative to the isolated gold and adsorbate species. [b]Au_{20} cluster models. [c]Au(111) periodic models. [d]Au_{13} cluster models.

length in break junction experiments.[86,97] The calculations also indicate that molecular assembly to form tightly packed films on functionalized nanoparticles occurs via diffusion of alkanethiolate−Au species, with significant particle resculpting possible in, for example, the wrapping of nanoparticles in multidentate molecules.[44,98]

Computational Design of Nanoparticle Arrays Based on Selective Replacement of Citrates by Dithiols on Gold Step Edges. Exploiting the intrinsic differences in site reactivity on nanoparticle surfaces is an attractive route to creation of interlinked nanoparticle arrays. We chose to study a di-isothiocyanate linker,[99] $Re_2(DMAA)_4(NCS)_2$ (Figure 5), which is soluble in acetone, a solvent which is miscible with water. Hence, for applications such as biosensing,[100] this linker has advantages over many of the molecules that are typically used for linking nanoparticles that are soluble only in nonpolar solvents.[101] The π-conjugated isothiocyanate end group also provides impedance smaller than that of methylene thiolate.[102] We use atomic scale calculations to study the formation of thiocyanate-linked citrate-protected gold nanoparticles (*n*-mer clusters). Following a similar protocol as described for the migration calculations above, three levels of atomic calculations are used to describe the nanoparticle−molecule−nanoparticle nanostructure, namely two types of electronic structure calculations followed by classical molecular dynamics simulations. First, two types of quantum mechanical models, molecular clusters and periodic surfaces, were used to compute the molecule−nanoparticle binding geometries and energies for both citrate−nanoparticle and linker−nanoparticle binding, over a range of different nanoparticle surface binding sites, some examples of which are shown in Figure 5. The combination of the molecular and periodic surface models allowed us to sample a wide range of different surface coordination states and also both bare and cation-complexed states for the citrate protector molecules. The adsorption geometries and energies obtained from the electronic structure calculations were used to create molecular dynamics models (Figure S22) to estimate counterion populations for the molecule−surface complexes in aqueous solution.

The use of both cluster and periodic models for the calculation of surface binding strengths allows a wide sampling of surface binding sites. In the instances in which different models were used to describe the same type of binding site, each model type gives a similar binding energy (Table 1). This allows direct qualitative comparison between binding strengths calculated for the different types of structurally inequivalent gold nanoparticle surface binding sites, ranging from coordinatively saturated terrace surface sites to progressively more coordinatively unsaturated step, ridge, and apex surface sites. For a typical size, 20 nm diameter, gold nanoparticle, there are in the region of 2 000 surface binding sites, defining a surface gold atom as one lying within the outer 3 Å shell of the nanoparticle and defining a molecule adsorption site as a 16-atom surface patch of gold atoms for both citrate and di-isothiocyanate molecules, consistent with STM images[103] and space-filling models. While the observed wide variation in shape and surface order/disorder for gold nanoparticles at this size range[104] makes it difficult to estimate the relative occurrence of each the representative surface binding site types, in general, the relative population of more coordinatively unsaturated sites will increase with decreasing nanoparticle diameter and may be expected to contribute strongly for nanoparticles with diameter on the order of 1−20 nm. The results of the binding energy calculations are shown in Table 1.

The computed binding energies show less stable adsorption modes for the bare citrate group as the degree of nanoparticle surface faceting increases, going from terrace surface sites to the more coordinatively unsaturated step, ridge, and apex surface sites. The alternative trisodium citrate state for the protector group shows similar destabilization at lower-coordination surface sites, though in this case the balance between decreased carboxylate−gold binding and enhanced carboxylate−sodium as well as sodium−gold binding gives a complex energy dependence with the lowest-coordinated apex site more stable than the intermediate edge site. Molecular dynamics models (Figure S22) show that the instantaneous citrate counterion state can vary between 0 and 3 over the full nanoparticle surface; therefore, citrate binding strengths will range from −0.5 to −1.6 eV, taking the sites in Table 1 as a representative sample of the available surface binding modes. Protecting groups bound to under-coordinated gold sites generally feature a lower population of sodium counterions, with short intercitrate distances on the nanoparticle surface allowing cations to be continuously exchanged between citrates as well as between carboxylates on each citrate. Water molecules mediate carboxylate−sodium−carboxylate charge networks and assist reshuffling of cations at the surface, with terrace sites in particular showing persistent ion pairing at the surface (Figure S22), over 24 ns of free dynamics, which may reduce the nanoparticle−nanoparticle repulsion. In reference vacuum simulations (not shown) in the absence of water, the full three-cation Na_3:citrate salt-type binding mode is preserved, as expected.

By contrast, the binding of the di-isothiocyanate linker molecule goes from a weak physisorption at terrace sites to stronger adsorption at more coordinatively unsaturated sites (Table 1). The surface curvature of the gold nanoparticles narrows the gap in adsorption energy between the protecting group and the functional linker, increasing the relative likelihood of binding of a linker molecule to the gold nanoparticle surface. In effect, the nanoparticle surface faceting penalizes binding of the trivalent citrate protector with its three carboxylates while favoring binding of the monovalent linker with its single isothiocyanate anchor per nanoparticle. Thus, we

believe that we have used the new data on gold atom site reactivities to design a potentially ideal means of creating interlinked gold nanoparticles (which could also provide, for example, ideal surface-enhanced Raman scattering (SERS) nanostructures for sensing and imaging applications),[105] and we hope that this design will be realized experimentally in the near future.

DISCUSSION

We compare our results with the findings of earlier and contemporaneous studies of hybrid organic−inorganic materials design and synthesis and discuss the relevance of our findings for the state of the art in realization of technologically useful molecule−metal contacts for molecular devices,[106] nanofabrication,[44,107] and molecular assembly.[108] Our conclusions are supported by additional data given in section 4.3 of Supporting Information, showing the negligible contribution from SAM molecule van der Waals packing energies for sub-20 carbon alkyl chain lengths and computed metal atom migration energies in alternatively shaped prolate gold clusters, platinum clusters, and gold and platinum grain boundaries.

Impact of Atom Migration on Metal−Molecule−Metal Contact Formation. We now discuss the energetics of migration and consequences for the assembly of molecule−metal−molecule junctions. The large computed barrier for complete unbinding and the significantly lower migration penalty supports the hypothesis that while there is substantial atomic reorganization at Au surfaces during electrode rupturing experiments or adsorption/desorption of molecules, there is conversely little true erosion of the surface whereby Au atoms would be fully dissociated when a molecule unbinds, e.g., upon molecular exchange in tunnel junctions or nanoparticle arrays.[8] The migratory "rolling" behavior may thus provide low barriers to reorganization while minimizing formation of permanent defects.

If one considers a typical molecular junction experiment (similarly, an electromigration experiment in which the Au atom motion is current-driven), a conductance plateau is observed upon pulling open a break junction. This plateau may conceivably be decomposed into two contributions: the conductance is approximately constant while the junction assembles with the anchor groups on the molecule sliding toward the apex of the electrodes, and the gold atoms may rearrange to optimize the contact. The calculated Au rolling behavior and the lowering of diffusion barriers for alkanethiolate−Au versus bare Au adatom species suggest motion of the Au atom at the surface in tandem with the motion of the molecule. By contrast, van der Waals unpacking of the molecule (+0.4 ± 0.1 eV and +0.3 ± 0.1 eV for octanethiol on 1 nm Au particles and Au(111), as described in section S4.3 of Supporting Information) has an energy penalty smaller than that of migration; therfore, the migration barrier is relevant. Figure S17 shows the linear dependence of molecule energies on chain length, calculated using van der Waals packing energies plus conformational energies in self-assembled monolayers on Au(111). The computed molecule-in-SAM energies indicate that the molecule unpacking energy will not outweigh the migration barrier, except in very long chain alkanes on very large nanoparticles (the transition is at $C_{20}H_{41}S$ for flat Au(111)). Very recent Monte Carlo models[109] showed slower diffusion in close-packed SAMs. To summarize, the molecule unbinding energies estimated by breaking van der Waals interactions between molecules in monolayers (Figure S17) and on nanoparticle surfaces (Figure S18) remain well below the energy required to unbind the molecule−Au species for all but very long chain alkanes that are rarely used in experiments. Thus, the highest barrier, the barrier relevant for experiment, is associated with molecule−gold, not free molecule, migration.

The unambiguous assignment of an experimental signature for coupled molecule and Au motion in the measured tunnel junction plateaus remains challenging, but the measured strength of approximately −1.7 eV for the Au−S bond[95] serves as an energetic payoff for the migration required for creation of, e.g., interlinked nanoparticle arrays.[8] We measured an activation energy, E_a, of 0.6 eV for junction formation (Figure 1c), which we rationalize by comparison with simulation models that indicate that this low barrier is consistent with Au−alkanethiolate diffusion on step edge features; migration of bare gold and migration from more coordinatively saturated surface sites have significantly larger barriers (Figure 3).

The calculated low-energy migration pathway also supports recent evidence that SAM surfaces contain a high concentration of mobile gold adatoms.[110−112] Both metal−molecule−metal junction and monolayer formation involve gold atom diffusion along gold substrates (i.e., migration via exchange between alternative partially bound states) rather than complete unbinding, so the ≤1 eV rather than 3 eV barrier is relevant. Indeed, a prudent choice of molecular junction may provide a means of minimizing gold atom migration; methylthiomethane for comparison has a binding energy on gold of only ∼0.5 eV[113] and so may diffuse as a free molecule rather than a molecule−Au moiety, but we are not aware of any such experimental tests to date. Note also that the Au atom migration pathway (Figure 4b) slopes downward toward larger displacements, by 50 meV/Å, which may drive the migration away from the initial binding site; this mild tendency may be strengthened (or opposed) by external electrical, chemical, and/or mechanical stresses in fabricated junctions. More generally, such a "liquid" model for the gold surface with low-barrier atomic migration provides a means for the electrode to taper and rearrange to optimize molecule−substrate contacts in the junction (with alkanethiolate−Au binding offsetting the Au migration penalty) while avoiding the extra +2 eV penalty for complete unbinding.

Comparison of Migration Energetics in Cluster and Periodic Models. The "rolling" migration pathway (Figure 4b) at +1.0 eV that arises spontaneously in the Au_{20} T_d cluster calculations shows a gold atom hopping out of the particle and rolling along the edge, leaving behind a vacancy defect on the surface. The energetics of this process are further discussed in section S3 of Supporting Information and are rationalized on the basis of coordination numbers for the unbinding atom and its vacancy site. Nevertheless, chemical intuition would suggest that it is more favorable for surface adatoms or atoms at monatomic step edges to migrate with fewer bonds being broken. Indeed, the computed migration barrier, E_b, of single Au atoms from low-coordination step edge and ridge sites on the Au(111) surface of +(0.7−0.8) eV are closer to the activation energy of 0.5−0.7 eV deduced from the experiments, with alkanethiolate bonding reducing the barrier further down into the range of the experimental E_a.

Finally, the computed migration barrier from grain boundaries formed between two Au_{20} clusters indicates a significantly lower cost for release of atoms from mismatched grain boundaries (section S4.6 of Supporting Information), which may trigger nanogap formation[114] at Au grain

boundaries. Pt particles, on the other hand, have stronger interatomic bonds and lower tendency to crack along grain boundaries (sections S4.4 and S4.5) and so may be expected to show a lower tendency for nanogap formation. This may in turn provide an opportunity for more controlled electromigration using Pt for the creation of gaps with better-defined geometry and hence more controllable electrical properties.

CONCLUSIONS

The present study provides insights in the atom-scale mechanisms underlying surface rearrangements in nanoscale molecular junctions. The computational data uses a combination of first-principles calculations of small gold nanoparticles (clusters) and periodic models of Au(111) surfaces and classical molecular dynamics simulations of molecule-coated gold. The models include a variety of different gold surface features including coordinatively saturated terrace sites and lower-coordination ridge, step edge, and apex sites. The simulations are used to explain the measured 0.6 eV activation energy associated with molecular exchange on gold nanoparticles, and the data is supported by a large set of control simulations that describe gold clusters in alternative geometries, defect clusters, and grain boundary effects in both gold and more tightly bonded platinum clusters. The experimentally validated computational methodology is then used to propose a means of creating interlinked nanoparticle arrays using programmed citrate replacement by thiocyanate linkers at step edges.

The present work considers the migration of single gold atom alkanethiolate−Au_1 species; future work could consider also the energetics of posited surface alkanethiolate−Au_2 species. It would be very interesting to compare migration barriers calculated for such alkanethiol−Au_2 models with the barriers obtained in the present study in which the cost for Au unbinding is shown to correlate with S−Au bond strength (Figure 3b,c). Hence, one may expect that the additional cost in unbinding energy for Au_2 from the underlying gold surface will be offset by stabilization of the migrating alkanethiolate−Au_2 species, and quantification of the net effect, if any (and comparison with the experimental E_a), would be useful for future molecular design studies. More advanced simulations, incorporating dynamic bond forming and breaking effects in molecular exchange and molecular surface dynamics (including Au−S bond switching and [115] formation and migration of other species such as alkanethiolate−Au_2 and alkanethiolate−Au−alkanethiolate moieties), may provide new information toward the eventual elucidation of the full mechanism of molecular exchange via coupled molecular and metal migration. For future experiments in molecular electronics, the ideal contact material may be a metal that can be quenched in order to stabilize the junction once formed, which may be possible in the future by manipulating the substrate atom migration barriers, molecule−substrate binding strengths, and molecule−molecule packing effects using different processing conditions and materials.

Selection of both molecule and metal is important, with, e.g., a mixed high/low-mobility Au/Pt alloy[116] providing a potential route to more reproducible junction assemblies. Ideal junctions would maximize the benefit of both the "liquid" Au for obtaining the most energetically favorable molecule−substrate geometries and the "solid" Pt for generating stable, long-lived metal−molecule−metal contacts.

ASSOCIATED CONTENT

The Supporting Information is available free of charge on the ACS Publications website at DOI: 10.1021/acs.jpcc.5b04383. Further experimental details; full description of simu- lation methods; further analysis of the unbinding pathways including modeling of defect clusters; frontier molecular orbitals of the low-barrier migration path; and discussion of the typical conditions involved in junction formation via molecular exchange, together with control simulations of migration on alternative prolate Au_{20} cluster geometries, migration on platinum clusters, and in both Au and Pt grain boundaries. (PDF) Movie of atom unbinding pathway for terrace site. (AVI) Movie of atom unbinding pathway for ridge site. (AVI) Movie of atom unbinding pathway for apex site. (AVI) Movie of low-barrier migration path. (AVI)

ACKNOWLEDGMENTS

D.T., A.J.Q., and M.C. acknowledge support from the European Community's 7th Framework Programme (FP7/2007-2013) under Grant 213382 (FUNMOL). D.T. thanks Science Foundation Ireland (SFI) for financial support under Grant 11/SIRG/B2111 and for provision of computing resources at the SFI/Higher Education Authority Irish Centre for High-End Computing (ICHEC). M.C. also acknowledges support from the European Commissions (EC) via the FP7 "'SYMONE'" 318597 and "'MOLESCO'" (ITN) 606728 projects. C.A.N. thanks the Singapore National Research Foundation (NRF) for support through Award NRF-CRP 8-2011-07.

REFERENCES

(1) Ho, P. S.; Kwok, T. Electromigration in Metals. *Rep. Prog. Phys.* 1989, *52*, 301−348.

(2) Park, H.; Lim, A. K. L.; Alivisatos, A. P.; Park, J.; McEuen, P. L. Fabrication of Metallic Electrodes with Nanometer Separation by Electromigration. *Appl. Phys. Lett.* 1999, *75*, 301−303.

(3) Champagne, A. R.; Pasupathy, A. N.; Ralph, D. C. Mechanically Adjustable and Electrically Gated Single-Molecule Transistors. *Nano Lett.* 2005, *5*, 305−308.

(4) Wu, S. M.; Gonzalez, M. T.; Huber, R.; Grunder, S.; Mayor, M.; Schonenberger, C.; Calame, M. Molecular Junctions Based on Aromatic Coupling. *Nat. Nanotechnol.* 2008, *3*, 569−574.

(5) Ulgut, B.; Abruna, H. D. Electron Transfer through Molecules and Assemblies at Electrode Surfaces. *Chem. Rev.* 2008, *108*, 2721−2736.

(6) Thurmer, D. J.; Bufon, C. C. B.; Deneke, C.; Schmidt, O. G. Nanomembrane-Based Mesoscopic Superconducting Hybrid Junctions. *Nano Lett.* 2010, *10*, 3704−3709.

(7) von Wrochem, F.; Gao, D. Q.; Scholz, F.; Nothofer, H. G.; Nelles, G.; Wessels, J. M. Efficient Electronic Coupling and Improved Stability with Dithiocarbamate-Based Molecular Junctions. *Nat. Nanotechnol.* 2010, *5*, 618−624.

(8) Liao, J. H.; Mangold, M. A.; Grunder, S.; Mayor, M.; Schonenberger, C.; Calame, M. Interlinking Au Nanoparticles in 2d Arrays Via Conjugated Dithiolated Molecules. *New J. Phys.* 2008, *10*, 065019.

(9) van der Molen, S. J.; Liao, J. H.; Kudernac, T.; Agustsson, J. S.; Bernard, L.; Calame, M.; van Wees, B. J.; Feringa, B. L.; Schonenberger, C. Light-Controlled Conductance Switching of Ordered Metal-Molecule-Metal Devices. *Nano Lett.* 2009, *9*, 76−80.
(10) Liao, J.; et al. Cyclic Conductance Switching in Networks of Redox-Active Molecular Junctions. *Nano Lett.* 2010, *10*, 759−764.
(11) Liao, J. H.; Blok, S.; van der Molen, S. J.; Diefenbach, S.; Holleitner, A. W.; Schonenberger, C.; Vladyka, A.; Calame, M. Ordered Nanoparticle Arrays Interconnected by Molecular Linkers: Electronic and Optoelectronic Properties. *Chem. Soc. Rev.* 2015, *44*, 999−1014.
(12) Sangeeth, C. S. S.; Wan, A.; Nijhuis, C. A. Equivalent Circuits of a Self-Assembled Monolayer-Based Tunnel Junction Determined by Impedance Spectroscopy. *J. Am. Chem. Soc.* 2014, *136*, 11134−11144.
(13) Tan, S. F.; Wu, L.; Yang, J. K. W.; Bai, P.; Bosman, M.; Nijhuis, C. A. Quantum Plasmon Resonances Controlled by Molecular Tunnel Junctions. *Science* 2014, *343*, 1496−1499.
(14) Sotthewes, K.; Wu, H. R.; Kumar, A.; Vancso, G. J.; Schon, P. M.; Zandvliet, H. J. W. Molecular Dynamics and Energy Landscape of Decanethiolates in Self-Assembled Monolayers on Au(111) Studied by Scanning Tunneling Microscopy. *Langmuir* 2013, *29*, 3662−3667.
(15) Bryant, B.; Renner, C.; Tokunaga, Y.; Tokura, Y.; Aeppli, G. Imaging Oxygen Defects and Their Motion at a Manganite Surface. *Nat. Commun.* 2011, *2*, 212.
(16) Xu, B. Q.; Tao, N. J. J. Measurement of Single-Molecule Resistance by Repeated Formation of Molecular Junctions. *Science* 2003, *301*, 1221−1223.
(17) Kaun, C. C.; Guo, H. Resistance of Alkanethiol Molecular Wires. *Nano Lett.* 2003, *3*, 1521−1525.
(18) Akkerman, H. B.; Blom, P. W. M.; de Leeuw, D. M.; de Boer, B. Towards Molecular Electronics with Large-Area Molecular Junctions. *Nature* 2006, *441*, 69−72.
(19) Fagas, G.; Delaney, P.; Greer, J. C. Independent Particle Descriptions of Tunneling Using the Many-Body Quantum Transport Approach. *Phys. Rev. B: Condens. Matter Mater. Phys.* 2006, *73*, 241314.
(20) Yuan, L.; Jiang, L.; Thompson, D.; Nijhuis, C. A. On the Remarkable Role of Surface Topography of the Bottom Electrodes in Blocking Leakage Currents in Molecular Diodes. *J. Am. Chem. Soc.* 2014, *136*, 6554−6557.
(21) Yuan, L.; Jiang, L.; Zhang, B.; Nijhuis, C. A. Dependency of the Tunneling Decay Coefficient in Molecular Tunneling Junctions on the Topography of the Bottom Electrodes. *Angew. Chem., Int. Ed.* 2014, *53*, 3377−3381.
(22) Dubi, Y. Transport through Self-Assembled Monolayer Molecular Junctions: Role of in-Plane Dephasing. *J. Phys. Chem. C* 2014, *118*, 21119−21127.
(23) Cucinotta, C. S.; Rungger, I.; Sanvito, S. First Principles Study of Electron Tunneling through Ice. *J. Phys. Chem. C* 2012, *116*, 22129−22138.
(24) Salomon, A.; Cahen, D.; Lindsay, S.; Tomfohr, J.; Engelkes, V. B.; Frisbie, C. D. Comparison of Electronic Transport Measurements on Organic Molecules. *Adv. Mater.* 2003, *15*, 1881−1890.
(25) Li, C.; Pobelov, I.; Wandlowski, T.; Bagrets, A.; Arnold, A.; Evers, F. Charge Transport in Single Au Vertical Bar Alkanedithiol Vertical Bar Au Junctions: Coordination Geometries and Conformational Degrees of Freedom. *J. Am. Chem. Soc.* 2008, *130*, 318−326.
(26) Kaliginedi, V.; Moreno-Garcia, P.; Valkenier, H.; Hong, W. J.; Garcia-Suarez, V. M.; Buiter, P.; Otten, J. L. H.; Hummelen, J. C.; Lambert, C. J.; Wandlowski, T. Correlations between Molecular Structure and Single-Junction Conductance: A Case Study with Oligo(Phenylene-Ethynylene)-Type Wires. *J. Am. Chem. Soc.* 2012, *134*, 5262−5275.
(27) Nijhuis, C. A.; Reus, W. F.; Barber, J. R.; Dickey, M. D.; Whitesides, G. M. Charge Transport and Rectification in Arrays of Sam-Based Tunneling Junctions. *Nano Lett.* 2010, *10*, 3611−3619.
(28) Kautz, N. A.; Kandel, S. A. Alkanethiol/Au(111) Self-Assembled Monolayers Contain Gold Adatoms: Scanning Tunneling Microscopy before and after Reaction with Atomic Hydrogen. *J. Am. Chem. Soc.* 2008, *130*, 6908.
(29) Kautz, N. A.; Kandel, S. A. Alkanethiol Monolayers Contain Gold Adatoms, and Adatom Coverage Is Independent of Chain Length. *J. Phys. Chem. C* 2009, *113*, 19286−19291.
(30) Raigoza, A. F.; Villalba, D. A.; Kautz, N. A.; Kandel, S. A. Structure and Self-Assembly of Sequentially Adsorbed Coronene/Octanethiol Monolayers. *Surf. Sci.* 2010, *604*, 1584−1590.
(31) Kautz, N. A.; Kandel, S. A. Reactivity of Self-Assembled Monolayers: Local Surface Environment Determines Monolayer Erosion Rates. *J. Phys. Chem. C* 2012, *116*, 4725−4731.
(32) Wu, H. R.; Sotthewes, K.; Kumar, A.; Vancso, G. J.; Schon, P. M.; Zandvliet, H. J. W. Dynamics of Decanethiol Self-Assembled Monolayers on Au(111) Studied by Time-Resolved Scanning Tunneling Microscopy. *Langmuir* 2013, *29*, 2250−2257.
(33) Vericat, C.; Vela, M. E.; Corthey, G.; Pensa, E.; Cortes, E.; Fonticelli, M. H.; Ibanez, F.; Benitez, G. E.; Carro, P.; Salvarezza, R. C. Self-Assembled Monolayers of Thiolates on Metals: A Review Article on Sulfur-Metal Chemistry and Surface Structures. *RSC Adv.* 2014, *4*, 27730−27754.
(34) Nirmalraj, P. N.; Schmid, H.; Gotsmann, B.; Riel, H. Nanoscale Origin of Defects at Metal/Molecule Engineered Interfaces. *Langmuir* 2013, *29*, 1340−1345.
(35) Gu, X.; Ji, M.; Wei, S. H.; Gong, X. G. Au-N Clusters (N = 32,33,34,35): Cagelike Structures of Pure Metal Atoms. *Phys. Rev. B: Condens. Matter Mater. Phys.* 2004, *70*, 205401.
(36) Bahn, S. R.; Jacobsen, K. W. Chain Formation of Metal Atoms. *Phys. Rev. Lett.* 2001, *87*, 266101.
(37) Kryachko, E. S.; Remacle, F. The Magic Gold Cluster Au(20). *Int. J. Quantum Chem.* 2007, *107*, 2922−2934.
(38) Strachan, D. R.; Johnston, D. E.; Guiton, B. S.; Datta, S. S.; Davies, P. K.; Bonnell, D. A.; Johnson, A. T. C. Real-Time TEM Imaging of the Formation of Crystalline Nanoscale Gaps. *Phys. Rev. Lett.* 2008, *100*, 056805.
(39) Prins, F.; Hayashi, T.; van Steenwijk, B. J. A. D.; Gao, B.; Osorio, E. A.; Muraki, K.; van der Zant, H. S. J. Room-Temperature Stability of Pt Nanogaps Formed by Self-Breaking. *Appl. Phys. Lett.* 2009, *94*, 123108.
(40) Molina, L. M.; Hammer, B. Theoretical Study of Thiol-Induced Reconstructions on the Au(111) Surface. *Chem. Phys. Lett.* 2002, *360*, 264−271.
(41) Jadzinsky, P. D.; Calero, G.; Ackerson, C. J.; Bushnell, D. A.; Kornberg, R. D. Structure of a Thiol Monolayer-Protected Gold Nanoparticle at 1.1 Angstrom Resolution. *Science* 2007, *318*, 430−433.
(42) Sudeep, P. K.; Emrick, T. Pearls of Wisdom: Stringing Nanoparticles and Polymers into New Assemblies and Materials. *ACS Nano* 2009, *3*, 2870−2875.
(43) Lopez-Acevedo, O.; Kacprzak, K. A.; Akola, J.; Hakkinen, H. Quantum Size Effects in Ambient Co Oxidation Catalysed by Ligand-Protected Gold Clusters. *Nat. Chem.* 2010, *2*, 329−334.
(44) Thompson, D.; Hermes, J. P.; Quinn, A. J.; Mayor, M. Scanning the Potential Energy Surface for Synthesis of Dendrimer-Wrapped Gold Clusters: Design Rules for True Single-Molecule Nanostructures. *ACS Nano* 2012, *6*, 3007−3017.
(45) Gronbeck, H.; Curioni, A.; Andreoni, W. Thiols and Disulfides on the Au(111) Surface: The Headgroup-Gold Interaction. *J. Am. Chem. Soc.* 2000, *122*, 3839−3842.
(46) Larsson, J. A.; Nolan, M.; Greer, J. C. Interactions between Thiol Molecular Linkers and the Au-13 Nanoparticle. *J. Phys. Chem. B* 2002, *106*, 5931−5937.
(47) Yin, K. L.; Xia, Q.; Xu, D. J.; Xi, H. T.; Sun, X. Q.; Chen, C. L. Computer Simulation of a Gold Nanoparticle Coated by Thiol-Terminated Hydroquinonyl Oligoethers. *Macromol. Theory Simul.* 2003, *12*, 593−598.
(48) Schmid, G.; Simon, U. Gold Nanoparticles: Assembly and Electrical Properties in 1−3 Dimensions. *Chem. Commun.* 2005, 697−710.
(49) Masens, C.; Ford, M. J.; Cortie, M. B. The Effect of Surface Symmetry on the Adsorption Energetics of Sch(3) on Gold Surfaces Studied Using Density Functional Theory. *Surf. Sci.* 2005, *580*, 19−29.

(50) Gonzalez, C.; Simon-Manso, Y.; Marquez, M.; Mujica, V. Chemisorption-Induced Spin Symmetry Breaking in Gold Clusters and the Onset of Paramagnetism in Capped Gold Nanoparticles. *J. Phys. Chem. B* 2006, *110*, 687−691.
(51) Singh, C.; Ghorai, P. K.; Horsch, M. A.; Jackson, A. M.; Larson, R. G.; Stellacci, F.; Glotzer, S. C. Entropy-Mediated Patterning of Surfactant-Coated Nanoparticles and Surfaces. *Phys. Rev. Lett.* 2007, *99*, 226106.
(52) Ghorai, P. K.; Glotzer, S. C. Molecular Dynamics Simulation Study of Self-Assembled Monolayers of Alkanethiol Surfactants on Spherical Gold Nanoparticles. *J. Phys. Chem. C* 2007, *111*, 15857−15862.
(53) Henz, B. J.; Hawa, T.; Zachariah, M. R. Mechano-Chemical Stability of Gold Nanoparticles Coated with Alkanethiolate Sams. *Langmuir* 2008, *24*, 773−783.
(54) Tian, P. Molecular Dynamics Simulations of Nanoparticles. *Annu. Rep. Prog. Chem., Sect. C: Phys. Chem.* 2008, *104*, 142−164.
(55) Gannon, G.; Greer, J. C.; Larsson, J. A.; Thompson, D. Molecular Dynamics Study of Naturally Occurring Defects in Self-Assembled Monolayer Formation. *ACS Nano* 2010, *4*, 921−932.
(56) Sikora, M.; Szymczak, P.; Thompson, D.; Cieplak, M. Linker-Mediated Assembly of Gold Nanoparticles into Multimeric Motifs. *Nanotechnology* 2011, *22*, 445601.
(57) Thompson, D.; Sikora, M.; Szymczak, P.; Cieplak, M. A Multi-Scale Molecular Dynamics Study of the Assembly of Micron-Size Supraparticles from 30 Nm Alkyl-Coated Nanoparticles. *Phys. Chem. Chem. Phys.* 2013, *15*, 8132−8143.
(58) Stobiecka, M.; Deeb, J.; Hepel, M. Ligand Exchange Effects in Gold Nanoparticle Assembly Induced by Oxidative Stress Biomarkers: Homocysteine and Cysteine. *Biophys. Chem.* 2010, *146*, 98−107.
(59) Mpourmpakis, G.; Caratzoulas, S.; Vlachos, D. G. What Controls Au Nanoparticle Dispersity During Growth? *Nano Lett.* 2010, *10*, 3408−3413.
(60) Mpourmpakis, G.; Vlachos, D. G. Insights into the Early Stages of Metal Nanoparticle Formation Via First-Principle Calculations: The Roles of Citrate and Water. *Langmuir* 2008, *24*, 7465−7473.
(61) Centrone, A.; Penzo, E.; Sharma, M.; Myerson, J. W.; Jackson, A. M.; Marzari, N.; Stellacci, F. The Role of Nanostructure in the Wetting Behavior of Mixed-Monolayer-Protected Metal Nanoparticles. *Proc. Natl. Acad. Sci. U. S. A.* 2008, *105*, 9886−9891.
(62) Kuna, J. J.; Voitchovsky, K.; Singh, C.; Jiang, H.; Mwenifumbo, S.; Ghorai, P. K.; Stevens, M. M.; Glotzer, S. C.; Stellacci, F. The Effect of Nanometre-Scale Structure on Interfacial Energy. *Nat. Mater.* 2009, *8*, 837−842.
(63) Liao, J. H.; Bernard, L.; Langer, M.; Schonenberger, C.; Calame, M. Reversible Formation of Molecular Junctions in Two-Dimensional Nanoparticle Arrays (Vol 18, Pg 2444, 2006). *Adv. Mater.* 2006, *18*, 2803−2803.
(64) Bernard, L.; Kamdzhilov, Y.; Calame, M.; van der Molen, S. J.; Liao, J. H.; Schonenberger, C. Spectroscopy of Molecular Junction Networks Obtained by Place Exchange in 2d Nanoparticle Arrays. *J. Phys. Chem. C* 2007, *111*, 18445−18450.
(65) Kresse, G.; Hafner, J. Abinitio Molecular-Dynamics for Liquid-Metals. *Phys. Rev. B: Condens. Matter Mater. Phys.* 1993, *47*, 558−561.
(66) Perdew, J. P.; Burke, K.; Ernzerhof, M. Generalized Gradient Approximation Made Simple. *Phys. Rev. Lett.* 1996, *77*, 3865−3868.
(67) Blochl, P. E. Projector Augmented-Wave Method. *Phys. Rev. B: Condens. Matter Mater. Phys.* 1994, *50*, 17953−17979.
(68) Rusu, P. C.; Brocks, G. Surface Dipoles and Work Functions of Alkylthiolates and Fluorinated Alkylthiolates on Au(111). *J. Phys. Chem. B* 2006, *110*, 22628−22634.
(69) Rusu, P. C.; Giovannetti, G.; Brocks, G. Dipole Formation at Interfaces of Alkanethiolate Self-Assembled Monolayers and Ag(111). *J. Phys. Chem. C* 2007, *111*, 14448−14456.
(70) Frisch, M. J. et al. *Gaussian 09*, revision A.1; Gaussian, Inc.: Wallingford, CT, 2009.
(71) Becke, A. D. Density-Functional Thermochemistry 0.3. The Role of Exact Exchange. *J. Chem. Phys.* 1993, *98*, 5648−5652.
(72) Periyasamy, G.; Remacle, F. Ligand and Solvation Effects on the Electronic Properties of Au-55 Clusters: A Density Functional Theory Study. *Nano Lett.* 2009, *9*, 3007−3011.
(73) Gruene, P.; Rayner, D. M.; Redlich, B.; van der Meer, A. F. G.; Lyon, J. T.; Meijer, G.; Fielicke, A. Structures of Neutral Au-7, Au-19, and Au-20 Clusters in the Gas Phase. *Science* 2008, *321*, 674−676.
(74) Varetto, U. MOLEKEL Version 4.3; Swiss National Supercomputing Centre: Manno, Switzerland.
(75) Schaftenaar, G.; Noordik, J. H. Molden: A Pre- and Post-Processing Program for Molecular and Electronic Structures. *J. Comput.-Aided Mol. Des.* 2000, *14*, 123−134.
(76) Humphrey, W.; Dalke, A.; Schulten, K. VMD: Visual Molecular Dynamics. *J. Mol. Graphics* 1996, *14*, 33−38.
(77) Beyer, M. K.; Clausen-Schaumann, H. Mechanochemistry: The Mechanical Activation of Covalent Bonds. *Chem. Rev.* 2005, *105*, 2921−2948.
(78) Wu, Z. M.; Steinacher, M.; Huber, R.; Calame, M.; van der Molen, S. J.; Schonenberger, C. Feedback Controlled Electromigration in Four-Terminal Nanojunctions. *Appl. Phys. Lett.* 2007, *91*, 053118.
(79) Keith, J. A.; Fantauzzi, D.; Jacob, T.; van Duin, A. C. T. Reactive Forcefield for Simulating Gold Surfaces and Nanoparticles. *Phys. Rev. B: Condens. Matter Mater. Phys.* 2010, *81*, 235404.
(80) Evangelakis, G. A.; Kallinteris, G. C.; Papanicolaou, N. I. Molecular Dynamics Study of Gold Adatom Diffusion on Low-Index Copper Surfaces. *Surf. Sci.* 1997, *394*, 185−191.
(81) Takano, J.; Takai, O.; Kogure, Y.; Doyama, M. Simulation of Atomic-Scale Surface Migration in Homoepitaxial Growth Using Embedded-Atom Method Potentials for Gold. *Thin Solid Films* 1998, *318*, 52−56.
(82) Zhang, W.; Sun, L. T.; Xu, Z. J.; Krasheninnikov, A. V.; Huai, P.; Zhu, Z. Y.; Banhart, F. Migration of Gold Atoms in Graphene Ribbons: Role of the Edges. *Phys. Rev. B: Condens. Matter Mater. Phys.* 2010, *81*, 125425.
(83) Dell'Angela, M.; et al. Relating Energy Level Alignment and Amine-Linked Single Molecule Junction Conductance. *Nano Lett.* 2010, *10*, 2470−2474.
(84) Gannon, G.; Larsson, J. A.; Greer, J. C.; Thompson, D. Quantification of Ink Diffusion in Microcontact Printing with Self-Assembled Monolayers. *Langmuir* 2009, *25*, 242−247.
(85) MacKerell, A. D.; et al. All-Atom Empirical Potential for Molecular Modeling and Dynamics Studies of Proteins. *J. Phys. Chem. B* 1998, *102*, 3586−3616.
(86) Huang, Z. F.; Xu, B. Q.; Chen, Y. C.; Di Ventra, M.; Tao, N. J. Measurement of Current-Induced Local Heating in a Single Molecule Junction. *Nano Lett.* 2006, *6*, 1240−1244.
(87) Li, J.; Li, X.; Zhai, H. J.; Wang, L. S. Au-20: A Tetrahedral Cluster. *Science* 2003, *299*, 864−867.
(88) Hakkinen, H. The Gold-Sulfur Interface at the Nanoscale. *Nat. Chem.* 2012, *4*, 443−455.
(89) Aradhya, S. V.; Frei, M.; Hybertsen, M. S.; Venkataraman, L. Van Der Waals Interactions at Metal/Organic Interfaces at the Single-Molecule Level. *Nat. Mater.* 2012, *11*, 872−876.
(90) Pei, Y.; Gao, Y.; Shao, N.; Zeng, X. C. Thiolate-Protected Au-20(Sr)(16) Cluster: Prolate Au-8 Core with New [Au-3(Sr)(4)] Staple Motif. *J. Am. Chem. Soc.* 2009, *131*, 13619−13621.
(91) Wang, H.; Leng, Y. Gold/Benzenedithiolate/Gold Molecular Junction: A Driven Dynamics Simulation on Structural Evolution and Breaking Force under Pulling. *J. Phys. Chem. C* 2015, *119*, 15216−15223.
(92) Heersche, H. B.; Lientschnig, G.; O'Neill, K.; van der Zant, H. S. J. In Situ Imaging of Electromigration-Induced Nanogap Formation by Transmission Electron Microscopy. *Appl. Phys. Lett.* 2007, *91*, 072107.
(93) Taychatanapat, T.; Bolotin, K. I.; Kuemmeth, F.; Ralph, D. C. Imaging Electromigration During the Formation of Break Junctions. *Nano Lett.* 2007, *7*, 652−656.
(94) Love, J. C.; Estroff, L. A.; Kriebel, J. K.; Nuzzo, R. G.; Whitesides, G. M. Self-Assembled Monolayers of Thiolates on Metals as a Form of Nanotechnology. *Chem. Rev.* 2005, *105*, 1103−1169.

(95) Ulman, A. Formation and Structure of Self-Assembled Monolayers. *Chem. Rev.* 1996, *96*, 1533−1554.
(96) Huang, Z. F.; Chen, F.; Bennett, P. A.; Tao, N. J. Single Molecule Junctions Formed Via Au-Thiol Contact: Stability and Breakdown Mechanism. *J. Am. Chem. Soc.* 2007, *129*, 13225−13231.
(97) Nef, C.; Frederix, P. L. T. M.; Brunner, J.; Schonenberger, C.; Calame, M. Force-Conductance Correlation in Individual Molecular Junctions. *Nanotechnology* 2012, *23*, 365201.
(98) Hermes, J. P.; Sander, F.; Fluch, U.; Peterle, T.; Thompson, D.; Urbani, R.; Pfohl, T.; Mayor, M. Monofunctionalized Gold Nanoparticles Stabilized by a Single Dendrimer Form Dumbbell Structures Upon Homocoupling. *J. Am. Chem. Soc.* 2012, *134*, 14674−14677.
(99) Lydon, D. P.; Spalding, T. R.; Gallagher, J. F. Substitution Reactions of Rhenium-Chloride Bonds in [Re-2(Dmaa)(4)Cl-2], (Dmaa = 2 ′,6 ′-Dimethylacetanilido); Synthesis and Characterisation of [Re-2(Dmaa)(4)X-2] (X = Nco, Ncs, N-3) and [Re-2(Dmaa)(4)L-N][Sbf6](2) (N = 2, L = Pyridine; N = 1, L = 4,4 ′-Bipyridine). *Polyhedron* 2003, *22*, 1281−1287.
(100) Sperling, R. A.; Rivera gil, P.; Zhang, F.; Zanella, M.; Parak, W. J. Biological Applications of Gold Nanoparticles. *Chem. Soc. Rev.* 2008, *37*, 1896−1908.
(101) Sperling, R. A.; Parak, W. J. Surface Modification, Functionalization and Bioconjugation of Colloidal Inorganic Nanoparticles. *Philos. Trans. R. Soc., A* 2010, *368*, 1333−1383.
(102) Fu, M.-D.; Chen, W. P.; Lu, H.-C.; Kuo, C.-T.; Tseng, W.-H.; Chen, C.-H. Conductance of Alkanediisothiocyanates: Effect of Headgroup-Electrode Contacts. *J. Phys. Chem. C* 2007, *111*, 11450−11455.
(103) Lin, Y.; Pan, G. B.; Su, G. J.; Fang, X. H.; Wan, L. J.; Bai, C. L. Study of Citrate Adsorbed on the Au(111) Surface by Scanning Probe Microscopy. *Langmuir* 2003, *19*, 10000−10003.
(104) Daniel, M. C.; Astruc, D. Gold Nanoparticles: Assembly, Supramolecular Chemistry, Quantum-Size-Related Properties, and Applications toward Biology, Catalysis, and Nanotechnology. *Chem. Rev.* 2004, *104*, 293−346.
(105) Lim, D. K.; Jeon, K. S.; Hwang, J. H.; Kim, H.; Kwon, S.; Suh, Y. D.; Nam, J. M. Highly Uniform and Reproducible Surface-Enhanced Raman Scattering from DNA-Tailorable Nanoparticles with 1-Nm Interior Gap. *Nat. Nanotechnol.* 2011, *6*, 452−460.
(106) Nerngchamnong, N.; Yuan, L.; Qi, D. C.; Li, J.; Thompson, D.; Nijhuis, C. A. The Role of Van Der Waals Forces in the Performance of Molecular Diodes. *Nat. Nanotechnol.* 2013, *8*, 113−118.
(107) Zhou, Y. H.; et al. A Universal Method to Produce Low-Work Function Electrodes for Organic Electronics. *Science* 2012, *336*, 327−332.
(108) Perl, A.; Gomez-Casado, A.; Thompson, D.; Dam, H. H.; Jonkheijm, P.; Reinhoudt, D. N.; Huskens, J. Gradient-Driven Motion of Multivalent Ligand Molecules Along a Surface Functionalized with Multiple Receptors. *Nat. Chem.* 2011, *3*, 317−322.
(109) Paulius, D.; Torres, D.; Illas, F.; Archibald, W. E. A Study on Adatom Transport through (Radical3 X Radical3)-R30 Degrees -Ch3s Self-Assembled Monolayers on Au(111) Using First Principles Calculations. *Phys. Chem. Chem. Phys.* 2014, *16*, 23067−73.
(110) Cossaro, A.; et al. X-Ray Diffraction and Computation Yield the Structure of Alkanethiols on Gold(111). *Science* 2008, *321*, 943−946.
(111) Voznyy, O.; Dubowski, J. J.; Yates, J. T.; Maksymovych, P. The Role of Gold Adatoms and Stereochemistry in Self-Assembly of Methylthiolate on Au(111). *J. Am. Chem. Soc.* 2009, *131*, 12989−12993.
(112) Wang, Z. W.; Palmer, R. E. Mass Spectrometry and Dynamics of Gold Adatoms Observed on the Surface of Size-Selected Au Nanoclusters. *Nano Lett.* 2012, *12*, 91−95.
(113) Lim, J. K.; Kim, I. H.; Kim, K. H.; Shin, K. S.; Kang, W.; Choo, J.; Joo, S. W. Adsorption of Dimethyl Sulfide and Methanethiolate on Ag and Au Surfaces: Surface-Enhanced Raman Scattering and Density Functional Theory Calculation Study. *Chem. Phys.* 2006, *330*, 245−252.
(114) Moth-Poulsen, K.; Bjornholm, T. Molecular Electronics with Single Molecules in Solid-State Devices. *Nat. Nanotechnol.* 2009, *4*, 551−556.
(115) Paulsson, M.; Krag, C.; Frederiksen, T.; Brandbyge, M. Conductance of Alkanedithiol Single-Molecule Junctions: A Molecular Dynamics Study. *Nano Lett.* 2009, *9*, 117−121.
(116) Xu, J. B.; Zhao, T. S.; Liang, Z. X.; Zhu, L. D. Facile Preparation of Aupt Alloy Nanoparticles from Organometallic Complex Precursor. *Chem. Mater.* 2008, *20*, 1688−1690.